Journal of Wind Engineering & Industrial Aerodynamics 234 (2023) 105327

Contents lists available at ScienceDirect

Journal of Wind Engineering & Industrial Aerodynamics

journal homepage: www.elsevier.com/locate/jweia

An integrated tool to improve the safety of seaports and waterways under strong wind conditions

A. Ricci [a,b,c,*], R. Vasaturo [b], B. Blocken [c,d]

[a] Department of Science, Technology and Society, University School For Advanced Studies IUSS Pavia, Pavia, Italy
[b] Building Physics and Services, Department of the Built Environment, Eindhoven University of Technology, Eindhoven, the Netherlands
[c] Building Physics and Sustainable Design, Department of Civil Engineering, KU Leuven, Leuven, Belgium
[d] Anemos BV Company, Spechtendreef 3, 2460 Lichtaart, Belgium

ARTICLE INFO

Keywords:
Seaport areas
Waterways
Local wind conditions
Integrated tool
CFD simulations
On-site measurements

ABSTRACT

The expanding capacity of seaports for worldwide competitiveness is leading to an increased risk exposure. The increasing ship size causes larger wind forces that can render ship navigation difficult in stormy weather. The alert system for the suspension of port operations is usually based on the wind conditions measured by anemometers installed (*i*) on top of cranes/buildings often sheltered for some wind sectors; hence unable to provide reliable wind statistics, (*ii*) at undisturbed positions (far from quays); hence unable to catch the actual wind near cranes/mooring ships. Despite many efforts towards the safety management of seaports and waterways, the prediction of real-time local wind conditions in such environments is still challenging. The goal of this paper is the innovative development of an integrated tool to transfer the measured wind field (by on-site measurements) from an undisturbed position to the sea lock under investigation by transfer coefficients computed with CFD. The tool allows tugboat pilots to check in real-time the mean wind speed, wind direction and turbulence intensity in the newly built *IJmuiden sea lock*, in the Netherlands. This project is targeted at improving the awareness of risks and the prevention of detrimental accidents in seaports in stormy weather.

1. Introduction

Coastal areas are among the most densely settled areas in the world (Neumann et al., 2015). Estimates indicate that approximately three billion people – about half of world's population – live within 200 km from a coastal line and by 2025 this number is likely to double (Population Reference Bureau, 2003). Seaports are important nodes that facilitate about 80% of the worldwide trade volume via sea (UNCTAD/RTM, 2018). In many cases they are considered the entry and the exit points of countries (Yip, 2008; Rodrigue and Notteboom, 2009; Wolfgang, 2013; Becker et al., 2015; Vairetti et al., 2019). The increasing globalization leads to a growing competition in global trade in which seaports, waterways, and in general all the involved port infrastructures play a key role (Cho et al., 2018; Sys et al., 2008; Gomez Paz et al., 2015). However, the expanding capacity of seaports for worldwide competitiveness and accommodating bigger cruise ships and containerships can lead to an increased risk exposure (Jian et al., 2019). On the one hand, the increasing ships size causes larger wind forces on the ships, which can render the ship navigation more complicated (International Transport Forum, 2015; Janssen et al., 2017); on the other hand, the complex port environment (e.g. buildings and cranes) can cause sheltering effects on moored ships and increase the uncertainty of wind load assessment (Ricci et al., 2020; Torre et al., 2021). Seaport areas, as a first point of contact between the sea and the inland, are already historically considered among the most vulnerable and risky in the world. In addition, nowadays they are increasingly threatened by climate change and natural disasters and catastrophes (Pelling, 2003; Leckebusch and Ulbrich, 2004; Ulbrich et al., 2009; UNCTAD, 2011; Cao and Lam, 2018; Kron et al., 2019). Here, accidents due to meteorological factors such as strong winds can lead to detrimental economic losses associated with negative consequences throughout the whole supply chain (Darbra and Casal, 2004; Ronza et al., 2009; Solari et al., 2012; Kron, 2013; Zhang and Lam, 2015, 2016).

The alert system for the suspension of port operations is usually based on the wind measured by anemometers installed (*i*) on top of cranes/buildings, which are often sheltered for some wind sectors and then unable to provide reliable wind statistics, or (*ii*) at undisturbed positions (far from quays) and then unable to catch the actual wind near

* Corresponding author. Department of Science, Technology and Society, Scuola Universitaria Superiore IUSS Pavia, Pavia, Italy.
E-mail addresses: alessio.ricci@iusspavia.it, a.ricci@tue.nl (A. Ricci), r.vasaturo@tue.nl (R. Vasaturo), bert.blocken@kuleuven.be (B. Blocken).

https://doi.org/10.1016/j.jweia.2023.105327
Received 31 August 2022; Received in revised form 16 November 2022; Accepted 22 January 2023
Available online 7 February 2023

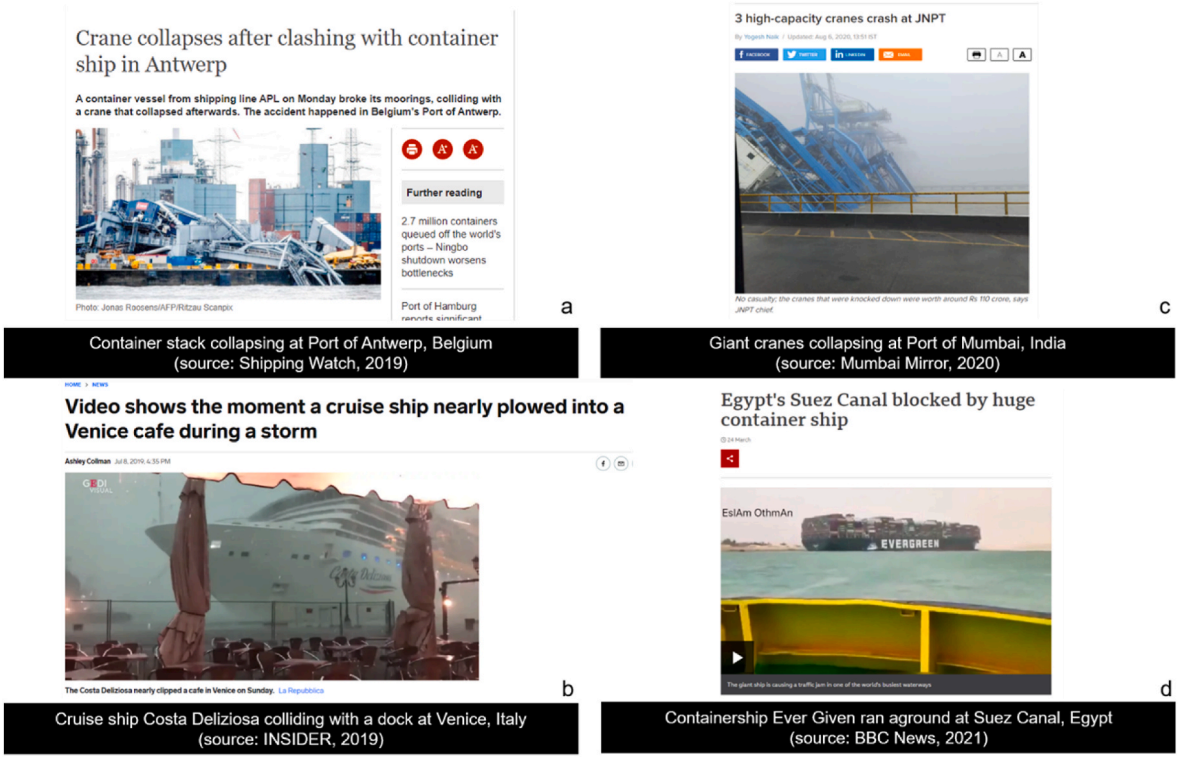

Fig. 1. Screenshots of newspaper article headlines reporting on accidents worldwide with cruise ships, containerships, container stacks and cranes under strong wind conditions.

cranes/mooring ships. In this regard, the recent years have seen a significant number of accidents involving cruise ships, containerships, and port infrastructures caused by strong winds in seaports and waterways. Some of these unfortunate events in recent years are reported here as an example: (1) on December 9, 2019, the containership *APL Mexico City* adrift hit and destroyed a crane at the Port of Antwerp (Belgium) (Shipping Watch, 2019) (Fig. 1a); (2) on July 8, 2019 the cruise ship *Costa Deliziosa* almost collided with the Giudecca Canal dock during a wind storm in Venice (Italy) (Insider, 2019) (Fig. 1b); (3) on August 5, 2020, giant cranes collapsed under strong wind conditions at the Port of Mumbai (India) (Mumbai Mirror, 2020) (Fig. 1c); (4) on March 23, 2021, the containership *Ever Given* ran aground in the Suez Canal (Egypt), one of the world's busiest waterways and the shortest shipping route between Europe and Asia (BBC News, 2021) (Fig. 1d).

A large amount of studies dealing with the risk and the interactions of hazard, exposure and vulnerability in coastal and seaport areas have been published in the past decades (e.g. Hsieh et al., 2014; Becker et al., 2015; Kolios et al., 2015; Taramelli et al., 2015; Mori and Takemi, 2016; Gharehgozli et al., 2017; van Dongeren et al., 2018; McIntosh and Becker, 2019). However, to the best knowledge of the authors, only a limited number of these focused on monitoring, modeling and characterizing the wind and/or waves by means of experimental and numerical methods. In the framework of two European projects, *Wind and Ports* (Solari et al., 2012; Burlando et al., 2014) and *Wind, Ports and Seas* (Repetto et al., 2017, 2018), the GS-WinDyn research group of the University of Genoa (Italy) developed an integrated web-based GIS platform (available to all port stakeholders) for the safe management and risk assessment of complex port areas exposed to strong winds. The platform is based on a wind monitoring network (i.e. anemometers and LiDARs), numerical codes for the multi-scale simulation of wind and wave fields (as the Weather Research & Forecasting, WRF), coupled with the wave model MIKE21 (Spectral Waves, Danish Hydrological Institute), wind and wave forecasting algorithms, and statistical wind climate analyses. Kortcheva et al. (2018) presented an innovative, fully automated marine system capable of providing real-time monitoring and analyses of historical data of wind, wave, storm-surge and oil spill drift. This system is based on numerical models and Information Communication Technology (ICT) tools for simulation of essential information, including warnings for marine extreme phenomena and hazards. Chen et al. (2020) carried out long-term shipboard measurements and numerical simulations to gain a better understanding of vessel performance in actual sea conditions and practical guidance for ship operations in rough sea conditions. Using meteorological and wave models, such as WRF and WAVEWATCH III (WW3), they carried out simulations of the weather and sea state for eight rough sea cases using grid datasets of the National Centers for the Environmental Prediction Final (NCEP-FNL) and European Center for Medium-range Weather Forecasts Interim Reanalysis (ERA-Interim). The results indicated that an optimum and safe ship route can be achieved with a high-resolution WRF model coupled to (*i*) NCEP-FNL initial and boundary conditions to generate ocean surface winds and (*ii*) the WW3 wave model to generate ocean surface waves in case of strong wind conditions. A significant number of publications dealing with data modeling, algorithms and Automatic Identification Systems (AIS) to simulate ship navigation in open sea, port areas and waterways without a direct measure and/or simulation of wind conditions, have also appeared in the past decades (e.g. Merrick et al., 2003; Almaz et al., 2006; Harati-Mokhtari et al., 2007; Bailey et al., 2008; Gunnar Aarsæther and Moan, 2009; Chen et al., 2015; Gao et al., 2015; Kang et al., 2019; Iseki, 2019; Rong et al., 2019; Zhou et al., 2020). However, despite many efforts towards the safety management of seaports and waterways, the accurate knowledge of local-scale wind conditions within such complex environments is still challenging. Even when numerical weather prediction (NWP) models (e.g. WRF and WINDS) are used in combination with on-site measurements, the results can suffer from major assumptions/limitations such as: (*i*) the coarse vertical and horizontal resolution of the computational grid (e.g. minimum grid size in the order of 80–100 m); (*ii*) the large simplifications of the obstacles (i.e. buildings, cranes and ships), which are never reproduced with their actual geometrical shapes and sizes, but in the best scenarios only implicitly in terms of increased aerodynamic

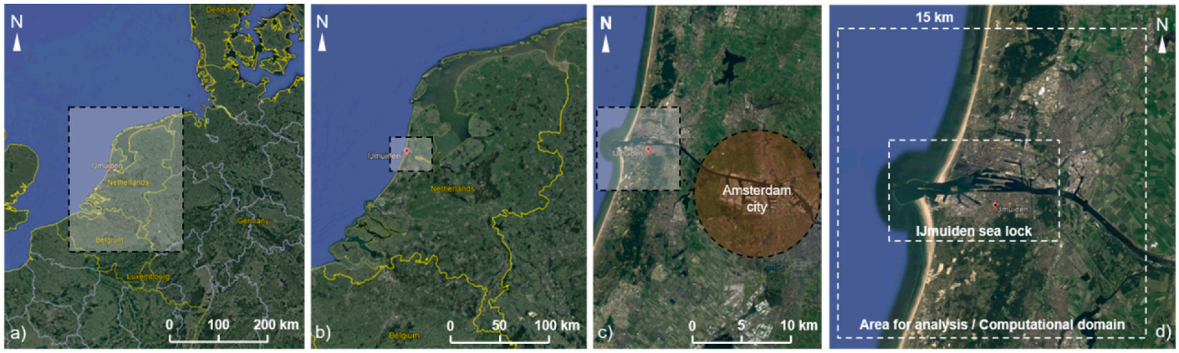

Fig. 2. Geographical location of the study area. Photo credit to *Google Maps*.

roughness lengths (z_0). Undoubtedly, numerical simulation with Computational Fluid Dynamics (CFD) in combination with on-site measurements can be a valuable approach to avoid these assumptions and overcome these limitations. Although the computational costs of CFD might be larger than NWP models (e.g. WRF and WINDS) to predict wind fields on the same mesoscale area because of the higher resolution of CFD geometries and grids to properly resolve the large-scale and local-scale wind effects induced by obstacles (e.g., Ricci et al., 2017, 2018), the CFD method has been widely applied in wind engineering research and practice (e.g., Stathopoulos, 2002; Hanjalic, 2005; Baker, 2007; Blocken, 2014, 2018). In this regard, besides its well-known limitations (Blocken, 2015), the steady Reynolds-averaged Navier--Stokes (RANS) has been shown to be sufficiently accurate to predict the high wind speed regions in ports (Ricci and Blocken, 2020) as well as wind forces on moored ships at quays (e.g. Ricci et al., 2020) and on isolated ships subjected to open sea-like wind conditions (e.g. Janssen et al., 2017; Prpic-Orsic et al., 2020; Hiroshi et al., 2022; Yoo et al., 2022).

In the present paper an integrated tool is innovatively developed to convert the measured wind field (by on-site measurements) from an undisturbed position to the sea lock under investigation by means of transfer coefficients obtained by RANS simulations. The RANS simulations and on-site measurements were presented in an earlier publication (Ricci and Blocken, 2020). The tool allows the tugboat pilots to check in real time the mean wind speed, wind direction and turbulence intensity in the newly built or new configuration of the *IJmuiden sea lock*, in the Port of Amsterdam (in the Netherlands) and its surrounding area. It should be noted that the methodology underlying the integrated tool and the conclusions of the present paper can also pertain to other complex seaports and waterways worldwide. The tool was designed in a

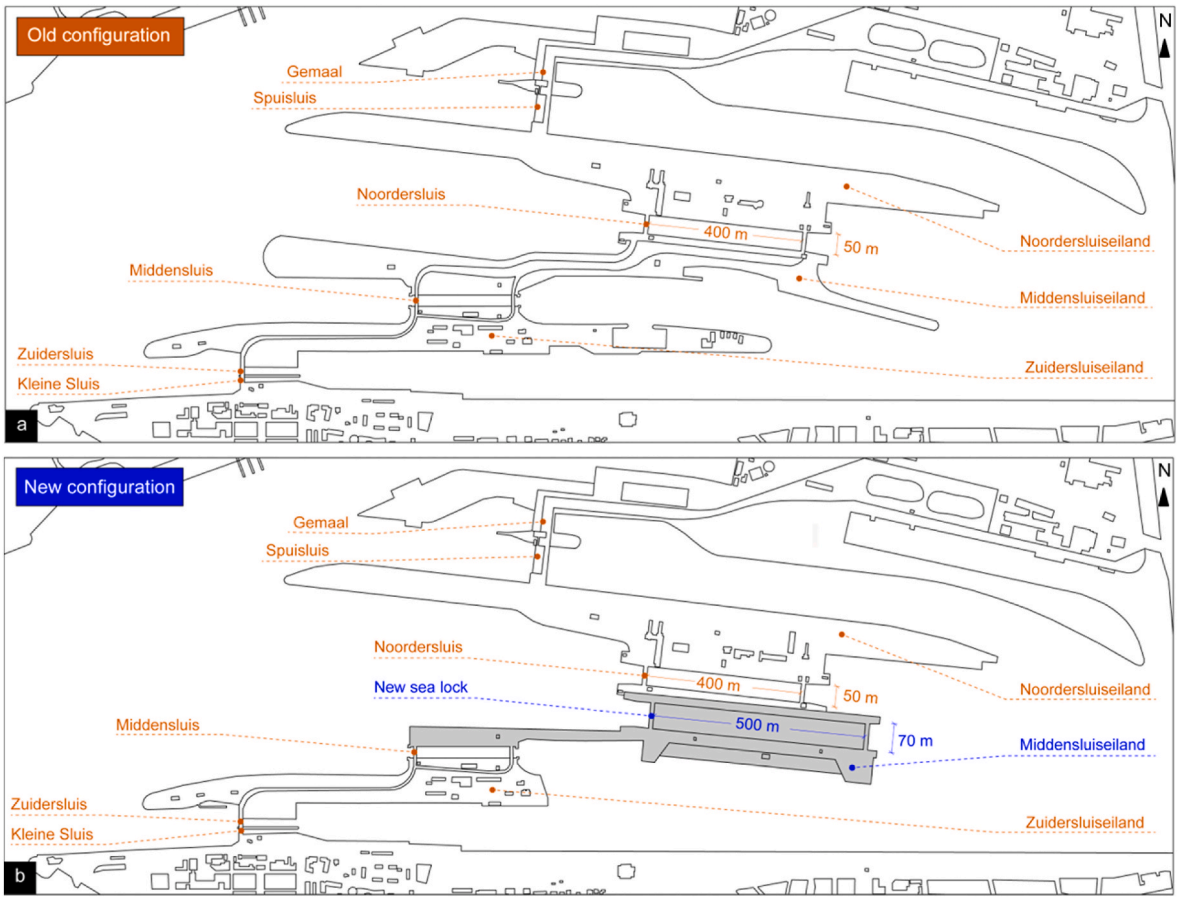

Fig. 3. Map of the IJmuiden sea lock: (*a*) *old configuration*; (*b*) *new configuration*.

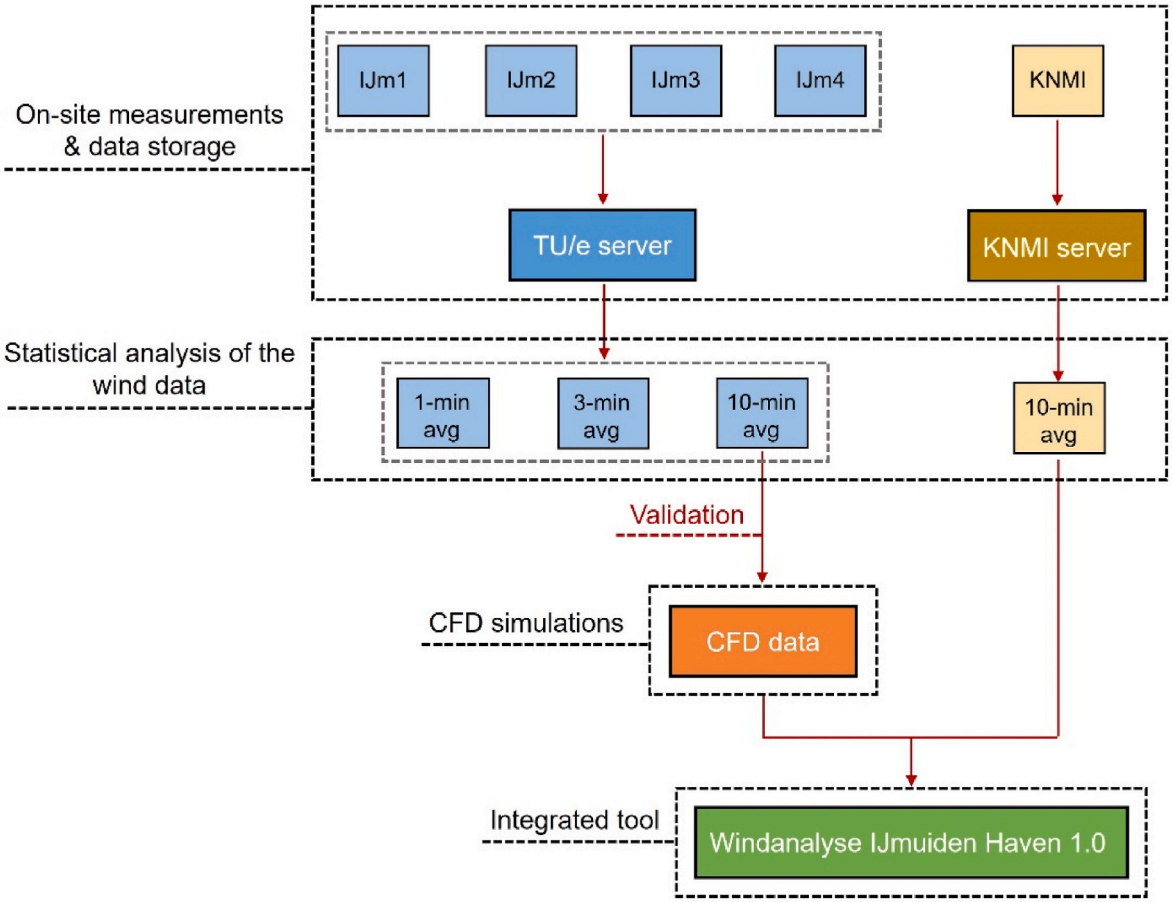

Fig. 4. Methodology of the present project and indication of the workflow.

research project carried out in cooperation with the Royal Netherlands Meteorological Institute (Koninklijk Nederlands Meteorologisch Instituut, KNMI) that provided the wind data of the reference anemometer station (see Section 3).

The paper is organized as follows: Section 2 describes the problem statement and the case study; in Section 3 the adopted methodology is described; in Section 4 a brief recap of the numerical and experimental analysis by Ricci and Blocken (2020) is provided; Section 5 describes the integrated tool *Windanalyse IJmuiden Haven 1.0*; Section 6 closes the paper with summary and conclusions.

2. The IJmuiden sea lock

The IJmuiden port is located at 40 km from Amsterdam (Netherlands) and it resides under the Port Authority of Amsterdam (Fig. 2a–d). The *IJmuiden sea lock* is a logistical hub specialized in the storage and transshipment of fertilizer and fossil fuels, agribulk, mixed cargo, building materials and recycling (Port of Amsterdam, New sea lock, 2021). The port also accommodates companies operating in the manufacturing industry and a large number of sea cruise liners. With more than 182 ocean-going cruise liners anchored in the Port of Amsterdam in 2015 and with 95 million tons of cargo handled in 2015, Amsterdam is the fourth largest European port, behind Rotterdam, Antwerp and Hamburg (KFW, 2021). However, as also stressed by the Maritime Security Regime Concept (2012) in the report *"A global approach to regional challenges"* published on September 2012, natural phenomena (as severe weather) may limit the access to ports and the trafficking between countries worldwide. Since these threats are expected to rise in the next years due to climate change (e.g. Pelling, 2003; Leckebusch and Ulbrich, 2004; Ulbrich et al., 2009; UNCTAD, 2011; Albers et al., 2015; Cao and Lam, 2018; Kron et al., 2019), it is important for port stakeholders to act in order to prevent major issues in the future. This was also one on the main reasons why, on January 2006, the Port Authority of Amsterdam together with the Directorate-General for Public Works and Water Management of the Netherlands announced the construction of the new longer, wider and deeper *sea lock* at the entrance of the North Sea Canal at the IJmuiden port (Port of Amsterdam, New sea lock, 2021). The project falls within the European program "Connecting Europe Facility" and is co-financed by the European Union (European Commission, 2021). The construction started in 2017 and should take about five years, so the new sea lock should be operative by the end 2022. It will be 500 m long, 70 m wide and 18 m deep and it will accommodate vessels of maximum 365 m in length, 57 m in width and 13.75 m in depth. The new sea lock will be 100 m longer, 20 m wider and 3 m deeper than the old Northern Lock, Noordersluis, which was one of the largest in the world in the year of its completion in 1929. The new sea lock not only differs from the Noordersluis in terms of size, it will also have a wider range of uses and will be tide-independent (Fig. 3a and b). The new sea lock will accommodate larger containerships and cruise ships daily crossing the entrance of the Port of Amsterdam. Although the design and construction of the new sea lock should generally enable safer and easier navigation throughout the whole sea lock, changes in wind speed and direction can still cause significant risks and potential associated damages for large ships maneuvering at the seaport and approaching the lock. Hence, for the tugboat pilots is essential to know the local wind conditions almost in real-time and throughout the whole area of action instead of only at some specific positions, which are commonly the entrance of the port where some anemometers are installed to detect the local undisturbed wind conditions. This was also the innovative goal the research project, in which an integrated tool -

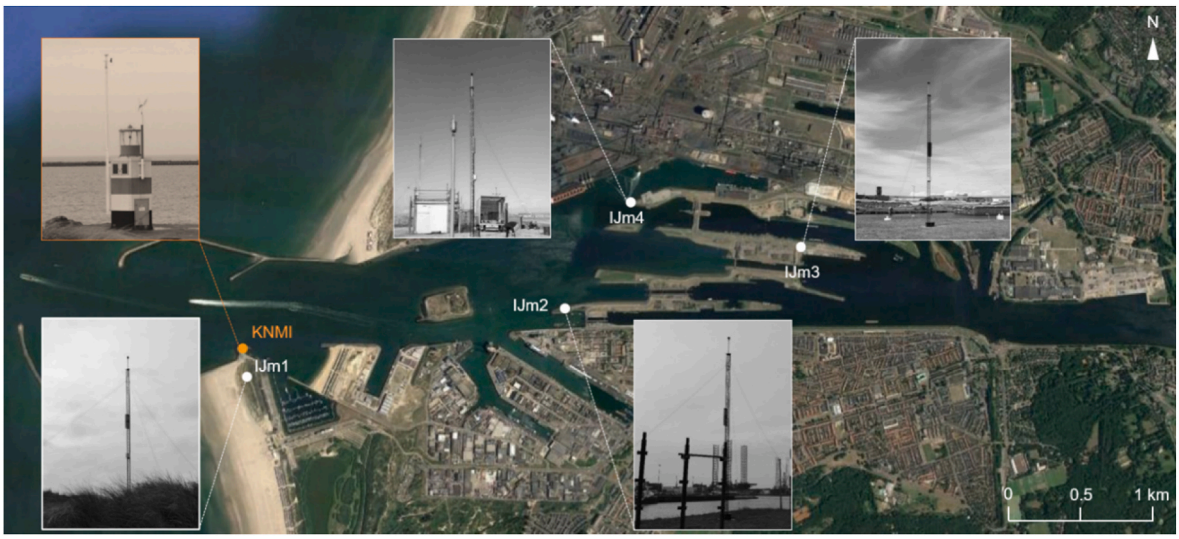

Fig. 5. Positions of the 2D ultrasonic anemometers (*IJm1*, *IJm2*, *IJm3* and *IJm4*) installed by Eindhoven University of Technology (TU/e) and the traditional cup anemometer (KNMI) of the Royal Netherlands Meteorological Institute (KNMI).

based on CFD simulations and on-site measurements - was developed. The tool has a twofold objective: (*i*) training the tugboat pilots based on the availability of the wind flow pattern throughout the whole sea lock in almost real-time; (*ii*) providing all port stakeholders with more insights in the local wind effects that can occur in the seaport area (Fig. 3b).

3. Methodology

The methodology adopted to develop the tool is illustrated in Fig. 4. The workflow was organized in four steps: the on-site measurements and data storage (Section 3.1), the statistical analysis of the wind data (Section 3.2), the CFD simulations and validation of the CFD data with the measured data (Section 3.3), and the development of the integrated tool for which an exhaustive description supported by illustrations is provided in Section 5.

3.1. On-site measurements and data storage

On-site measurements were carried out with five 2D ultrasonic anemometers (*IJm1*, *IJm2*, *IJm3*, *IJm4, KNMI*) applying a sampling frequency of 1 Hz (Fig. 5). The stations *IJm1*, *IJm2*, *IJm3* and *IJm4* were installed at a height of about 15 m above mean sea level (MSL) and measurements were performed for a duration of one year (i.e. July 5, 2017–July 1, 2018). One-year measurements is commonly considered by Wind Engineering and Atmospheric Sciences experts a sufficient time to gather a wider number of wind data necessary to characterize the wind through any seasonal variation. At the end of the measurement period, the four ultrasonic anemometers of TU/e were removed. The station named *KNMI*, property of the KNMI, is permanently installed in the study area and was already present when the four additional anemometers by Eindhoven University of Technology (TU/e) were installed (Fig. 5). The *KNMI* station consisted of traditional measurement equipment, i.e. a cup anemometer and a wind vane, and for this reason the *IJm1* station with a more sophisticated equipment was installed nearby the *KNMI* station (Fig. 5). Since from the historical wind data of the *KNMI* station, the wind at this location appeared to be not significantly influenced by the immediate surroundings, as also confirmed by the results provided in a previous publication (see also Ricci and Blocken, 2020), the *KNMI* and *IJm1* stations were chosen as reference stations. The stations *IJm1-4* better equipped (consequently more accurate) than the *KNMI* station were used to validate the CFD results by Ricci and Blocken (2020), but since these stations were removed at the end of the measurement period, they were not used explicitly in the development of the tool. Conversely, the *KNMI* station permanently installed there (as opposed to *IJm1* installed there only for one year) was not considered for the validation step, but only used for transferring the measured wind speed and direction from the undisturbed position to every location of the sea lock, both during the tool development and after the completion of the project for training the tugboat pilots. The anemometers installed by TU/e were mounted on truss masts and equipped with a data logger to locally store the data with the frequency of 1Hz on a SD card. Then collected data were sent with the same frequency to the TU/e server, located at the Building and Physics and Services laboratory at the TU/e campus, by a Wi-Fi connection (Fig. 4). The TU/e stations were supplied by a battery chargeable with a small photovoltaic panel installed on a side of the truss mast. The TU/e and KNMI databases were safely protected and the two servers were reachable only by its assigned users. The TU/e team was allowed to read the KNMI 10-min average wind statistics only for the last 24 h of measurements by means of a File Transfer Protocol (FTP) server, which provided data every 10 min.

3.2. Statistical analysis of the wind data

The wind data collected from stations *IJm1*, *IJm2*, *IJm3* and *IJm4* were post-processed. A database composed of 1-min, 3-min and 10-min average wind speed (U), wind direction (φ) and turbulence intensity (I) was analyzed in order to identify possible neutral stability atmospheric boundary layer (ABL) conditions (Stull, 1988). In accordance with the atmospheric stability classes proposed by Pasquill (1961) and in absence of temperature data, only strong wind conditions (i.e. with 10-min average wind speed values greater than 6 m/s) - regarded as potentially dangerous for ships operations in port areas - were considered to validate the CFD results, assuming that the thermal effects in these ABL flows were negligible. The present dataset (of *IJm2*, *IJm3* and *IJm4*) was exclusively used to validate the CFD results (see also Ricci and Blocken, 2020) and not as input for the integrated tool presented in this paper. During the period of the measurements (i.e. July 5, 2017–July 1, 2018), two exceptional storm events occurred on 3 and January 18, 2018, causing technical damage to the stations *IJm2* and *IJm3* with a subsequent disruption of the network system and loss of data for several days. Thus, these extreme events could not be considered for the validation of the CFD simulations. On January 18, 2018 strong winds with peak wind speeds of about 42 m/s registered at the Port of Rotterdam (Hoek van Holland) occurred along the coasts of Netherlands, Belgium and the North-West coast of Germany. The storm lasted about 3 hours and was

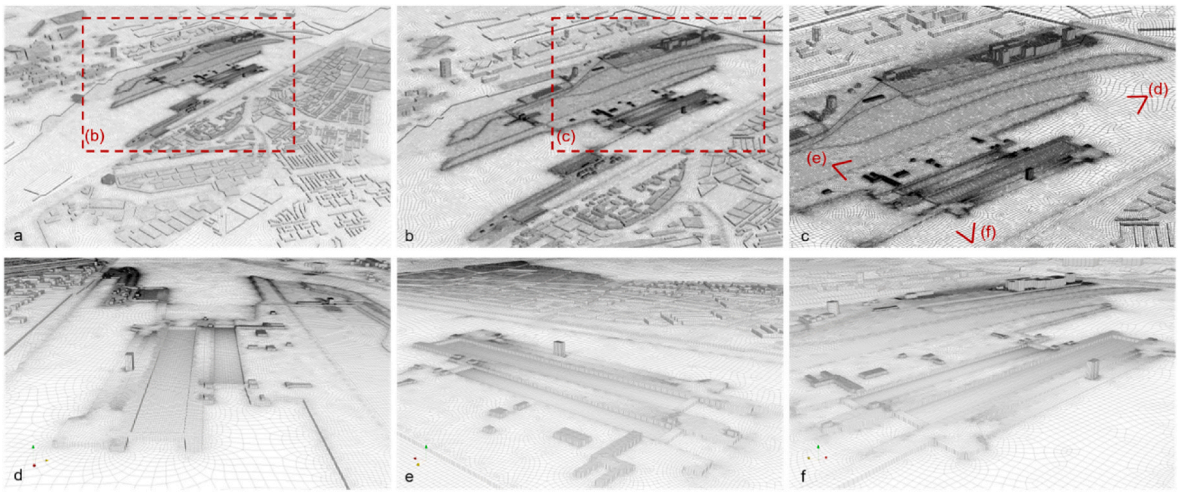

Fig. 6. Computational grid of the *new configuration* of the *IJmuiden sea lock* in different perspective views: (*a-c*) South-West view; (*d*) East view; (*e*) North-West view; (*f*) South-South-West view. Total cell count is 74 million.

classified by the KNMI as one of the toughest storms hitting the Netherlands in the recent 50 years (KNMI, 2018). The storm caused serious problems to a large part of the country: overturned containers in the main seaport areas (e.g. Port of Rotterdam), traffic of trains was stopped, numerous highways closed, more than 300 flights were canceled, and three people died (BBC News, 2018; HetLegioen, 2018).

3.3. CFD simulations

3D steady RANS simulations with closure by the realizable k-ε turbulence model (Shih et al., 1995) were carried out for 24 reference wind directions (θ) to cover the whole wind rose. The computational domain, covering an area of 15 km^2 (i.e. $L \times L = 15 \times 15$ km^2) with a height of 0.5 km, was chosen much larger than the area of interest (of about 3 × 8 km^2, see Fig. 5) to allow the ABL wind to fully develop (Blocken et al., 2007a,b; Vasaturo et al., 2018) over the seaport area. The high-resolution computational grid was built using the surface-grid extrusion technique (van Hooff and Blocken, 2010) and counted approximately 74 million hexahedral and prismatic cells. Fig. 6 provides an overview of the computational grid with different perspective views. The best practice guidelines for CFD application in wind engineering were adopted to construct the computational domain and grid (Casey and Wintergerste, 2000; Britter and Schatzmann, 2007; Blocken and Gualtieri, 2012; Blocken, 2015; Franke et al., 2007; Tominaga et al., 2008). The aerodynamic roughness length (z_0) values, to be imposed at the bottom of the domain using patches of about equal roughness, were defined in accordance with the Davenport classification modified by Wieringa (1992) (Fig. 7). Therefore, the z_0 values were converted into corresponding equivalent sand-grain roughness height (k_s) values using the standard wall functions by Launder and Spalding (1974) with roughness modification by Cebeci and Bradshaw (1997) and the relationship between z_0, k_S and the roughness constant C_S derived by Blocken et al. (2007a) for the commercial code ANSYS Fluent. All simulations were carried out with ANSYS Fluent 16.0 (ANSYS Fluent, 2013). The details about the computational domain, grid and other settings can be found in Ricci and Blocken (2020). The CFD results (simulated data) were validated with the measured data in terms of the wind speed amplification factor (K), the turbulence intensity amplification factor (Y), and the local wind direction (φ), for 24 reference wind directions. It is worth to mention that CFD simulations were not run based on the 1-year measurements, but simply validated based on them. It means that even if slightly different wind conditions may occur in the next years, the CFD model would be able to hold such variations as long as they belong to neutral ABL conditions.

The simulated data were used to develop the integrated tool that works with the data from the *KNMI* station as input. The entire procedure is described in Section 5.

4. Validation of CFD results

A brief recap of the validation study related to *step 3*, fully described in the earlier publication by Ricci and Blocken (2020), is reported in the present section to aid the reader in understanding the development of the integrated tool.

Fig. 8 summarizes the comparison between the measured and simulated data in terms of wind speed amplification factor (K_{exp} and K_{num}), local wind direction (φ_{exp} and φ_{num}) and turbulence intensity amplification factor (Y_{exp} and Y_{num}), for the 24 reference wind directions at the four positions (*IJm1*, *IJm2*, *IJm3* and *IJm4*). The amplification factor (K) is defined as the ratio between the mean wind speed (U) at the measurement position (e.g. at *IJm2*, *IJm3* and *IJm4*) and the reference mean wind speed (U_{ref}) at *IJm1*. Similarly, the turbulence intensity amplification factor (Y) was defined as the ratio between the local mean turbulence intensity I at the measurement position (e.g. at *IJm2*, *IJm3* and *IJm4*) and the reference mean value I_{ref} at *IJm1*. For the measured data, the 10-min average wind speed and turbulence intensity were considered for U, U_{ref}, I and I_{ref}.

For K (Fig. 8a), a satisfactory agreement was found with about 90% of the simulated data within ±30% from the measured data, on a database of 72 samples. Deviations larger than 30% were found for four reference wind directions: 105°, 120°, 330° and 345°. For $\theta = 105°$, an overestimation by K_{num} was found at *IJm2*, *IJm3* and *IJm4*. For $\theta = 120°$, overestimations by K_{num} were found at *IJm3* and *IJm4*. For $\theta = 330°$ and $\theta = 345°$, overestimations by K_{num} were observed at *IJm4* and *IJm3*, respectively.

For φ (Fig. 8b), generally a narrow distribution around the diagonal was observed with about 90% of φ_{num} within ±30° of deviation with respect to φ_{exp}, on a database of 96 samples. At the reference station *IJm1* the agreement between φ_{exp} and φ_{num} was within ±5° of deviation. Conversely, some deviations larger than ±30° were found at the other three stations for specific wind directions. At *IJm2* and *IJm3*, underestimations by φ_{num} were found for $\theta = 15°$ and in the wind sector 105°-120. In contrast, at *IJm3* and *IJm4* overestimations by φ_{num} were found for $\theta = 345°$ and in the wind sector 330°–345°, respectively.

For Y (Fig. 8c), a less satisfactory agreement was obtained between simulations and measurements with about 74% of Y_{num} within ±30° with respect to the Y_{exp}, on a database of 72 samples. For a large number of reference wind directions (i.e. about 50% of the total) the stations

Fig. 7. Aerodynamic roughness length (z_0), roughness constant (C_S) and equivalent sand-grain roughness height (k_S) for patches with different terrain roughness categories.

IJm2, *IJm3*, *IJm4* are shielded by the surrounding buildings leading to extensive wake flow zones in the middle of the sea lock. The inaccuracy of the 3D steady RANS approach in predicting the wake flow possibly caused mainly some underestimations as well as some overestimations by Y_{num}.

In accordance with previous similar studies (e.g. Blocken et al., 2015; Ricci et al., 2020; Ricci et al., 2022), the 3D steady RANS approach showed a generally high reliability to predict the local wind conditions in the *IJmuiden sea lock*, especially in high wind speed amplification factor regions (Blocken, 2018). These are usually also the regions that are considered in combination among the most risky and dangerous conditions for ship navigating throughout narrow waterways and seaports (Darbra and Casal, 2004; Torre et al., 2021).

5. The integrated tool *Windanalyse IJmuiden Haven 1.0*

The goal of the developed tool was to make mean wind speed, wind direction and turbulence information for ship navigation in the *IJmuiden sea lock* readily available at every location and in almost real-time to help the tugboat pilots and the Port Authority of Amsterdam in safely guiding container ships, cruise ships and vessels throughout the sea lock. The general framework of the tool is based on the on-site measurements and the CFD data already described in Section 3 and recapitulated in Fig. 9. More details about the architecture of the tool, the algorithm and the code are provided in Section 5.1 and Fig. 9, while the graphical interface is fully described and illustrated in Section 5.2.

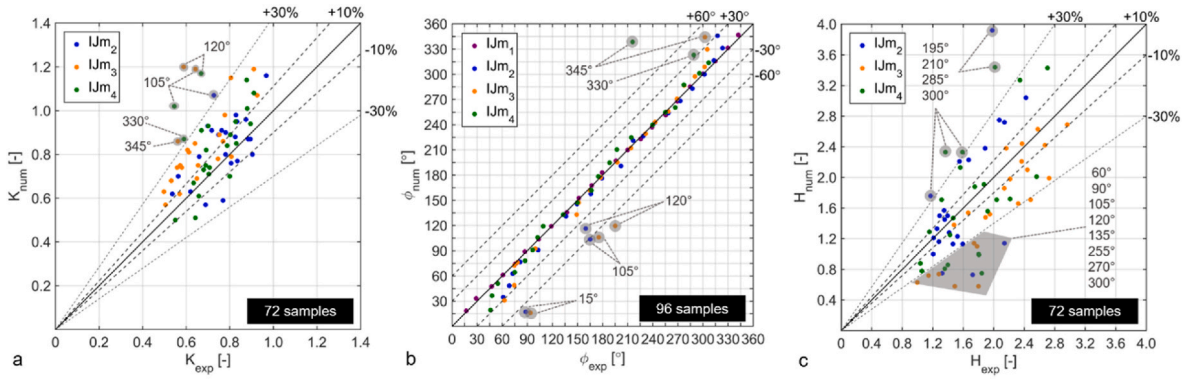

Fig. 8. Comparison of simulated and measured data at 15 m above MSL at the measurement positions for 24 reference wind directions (θ): (*a*) wind speed amplification factor (K), (*b*) local wind direction (φ), (*c*) and turbulence intensity amplification factor (Y). The number of samples and the values of K, φ and Y with deviations between CFD and experiments exceeding 30%, 30° and 60°, respectively, are also indicated in the figures.

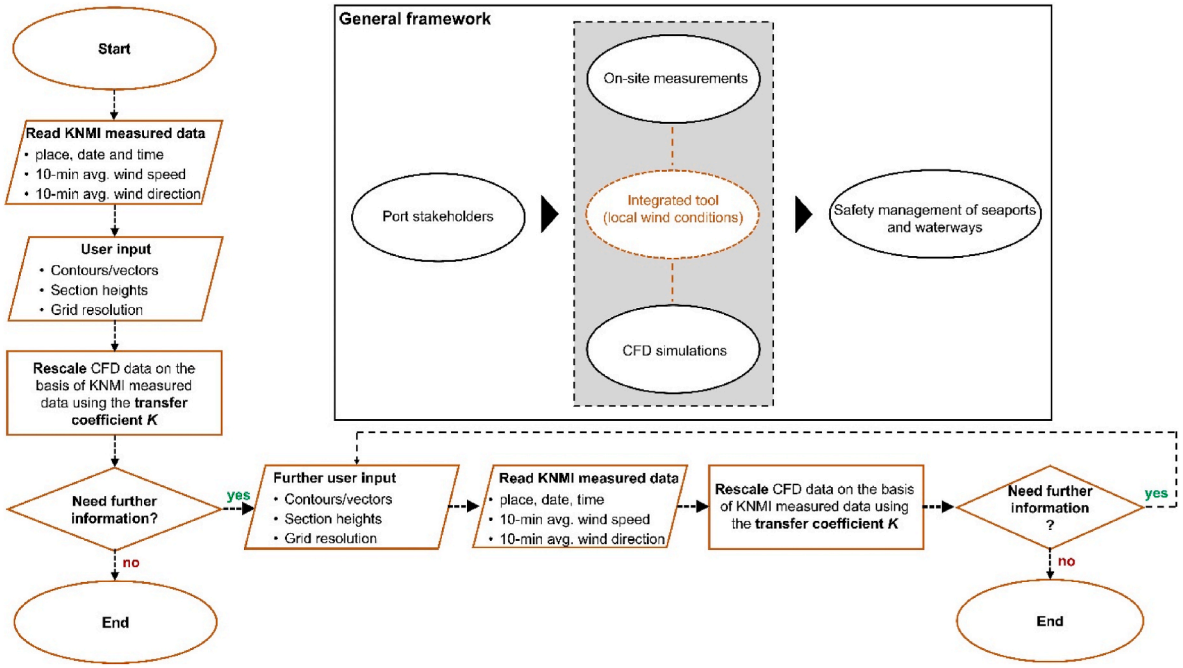

Fig. 9. General framework of the research project and architecture of the integrated tool *Windanalyse IJmuiden Haven 1.0*.

5.1. The architecture of the integrated tool

The tool was developed using MATLAB® 9.4 (release 2016b) and the MATLAB Compiler™; it can be run as a standalone application by installing MATLAB Runtime libraries (Mathworks, 2016). As illustrated in Fig. 9, the tool design was based on a straightforward principle for which the validated 3D steady RANS results, for 24 reference wind directions ($\theta = 0°, 15°, \ldots, 345°$) (see also Section 3), were linearly scaled according to the 10-min average wind speed (U) measured by the *KNMI* station ("Read KNMI measured data" blocks in Fig. 9), the only station permanently installed in the study area and available for providing real-time data. These wind data were downloaded from the KNMI website via FTP server, as previously described in Section 3. In order to build the tool, CFD data (mean velocity, wind direction, turbulence intensity and amplification factors) were first collected (as .csv files) along horizontal planes at different heights (10, 20 and 40 m) from the 24 simulated wind directions (θ). Although CFD simulations were performed over an area of 15 × 15 km^2, only the area of interest including the new sea lock (of about 3 × 8 km^2, see Fig. 5) was considered in the tool to comply with the explicit requests of the client, i.e. the Port Authority of Amsterdam. These data were pre-processed in MATLAB to build a database to be used in the standalone tool. The data were interpolated from an unstructured grid (CFD) to a regularly spaced domain (MATLAB) using the MATLAB function *TriScatteredInterp* and stored in .mat files as matrices. The two spatial resolutions were 5 and 10 m, corresponding with matrix dimensions of 738 × 1640 and 369 × 820, respectively. As a result, the .mat files database was eventually composed of 432 files, which were statically included in the standalone tool.

A transfer coefficient (Burlando et al., 2010, 2013) was calculated in order to linearly scale the CFD data according to the 10-min average wind speed (U) measured by the *KNMI* station. The transfer coefficient ($\boldsymbol{K_i}$) – also called amplification factor in the validation study (see Section 3) – was defined from the 3D steady RANS simulations and for the *i-th* wind direction, as follows (Equation (1)):

$$\boldsymbol{K_i} = \frac{1}{U_{KNMI,i \mid CFD}} \boldsymbol{U_{i \mid CFD}} \tag{1}$$

The CFD values were finally rescaled ("Rescale […] using the transfer coefficient K" blocks in Fig. 9) based on the 10-min averaged

Fig. 10. Screenshot of the *Home* interface of the integrated tool *Windanalyse IJmuiden Haven 1.0*.

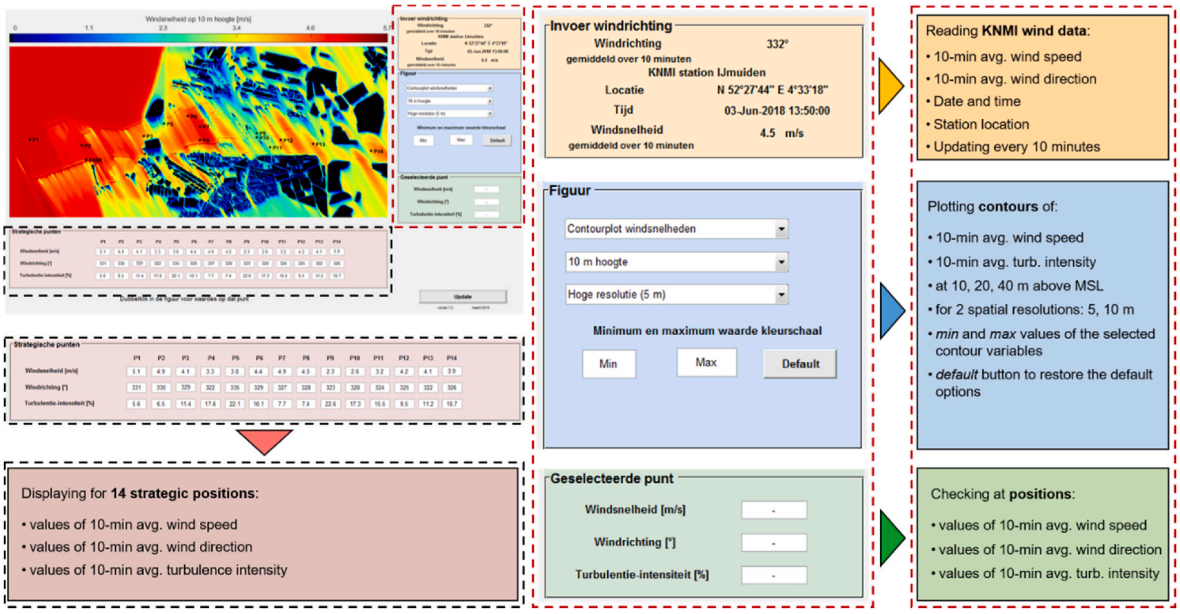

Fig. 11. Description of individual functions of *Windanalyse IJmuiden Haven 1.0* translated from Dutch (the original language of the tool) to English.

wind speed ($\overline{U_{KNMI}}$) measured at the *KNMI* station (read every 10 min by the tool), as follows (Equation (2)):

$$\boldsymbol{U}_i = \overline{U_{KNMI}}\,\boldsymbol{K}_i \tag{2}$$

It is important to note that also $\boldsymbol{U}_i$ is a matrix. Since the real-time measured wind direction at the *KNMI* station (*Invoer windrichting* in Fig. 10) is (obviously) not necessarily a multiple of 15°, the data employed for rescaling are those referred to the CFD simulation whose wind direction is the closest multiple of 15° (e.g. if the real-time *KNMI* wind direction is 67°, CFD data from the simulation with the wind direction of 60° are employed). Although this can be considered as a limitation, an error of ±7.5° is still considered minor given the complexity of the seaport topography and the turbulent ABL flow. Although included in the software, the turbulence intensity was not rescaled according to measured data, since it was not explicitly requested by the KNMI as real-time output to support the tugboat pilots who are mainly interested in the wind speed and wind direction. The resulting application is finally built using the MATLAB Compiler™ and then zipped. The total software tool size is about 1 GB, mostly occupied by the large CFD database. *Windanalyse Ijmuiden Haven 1.0* can be easily installed (a "readme.txt" file is provided) and launched as standalone application; downloading the freely available MATLAB Runtime libraries is also required.

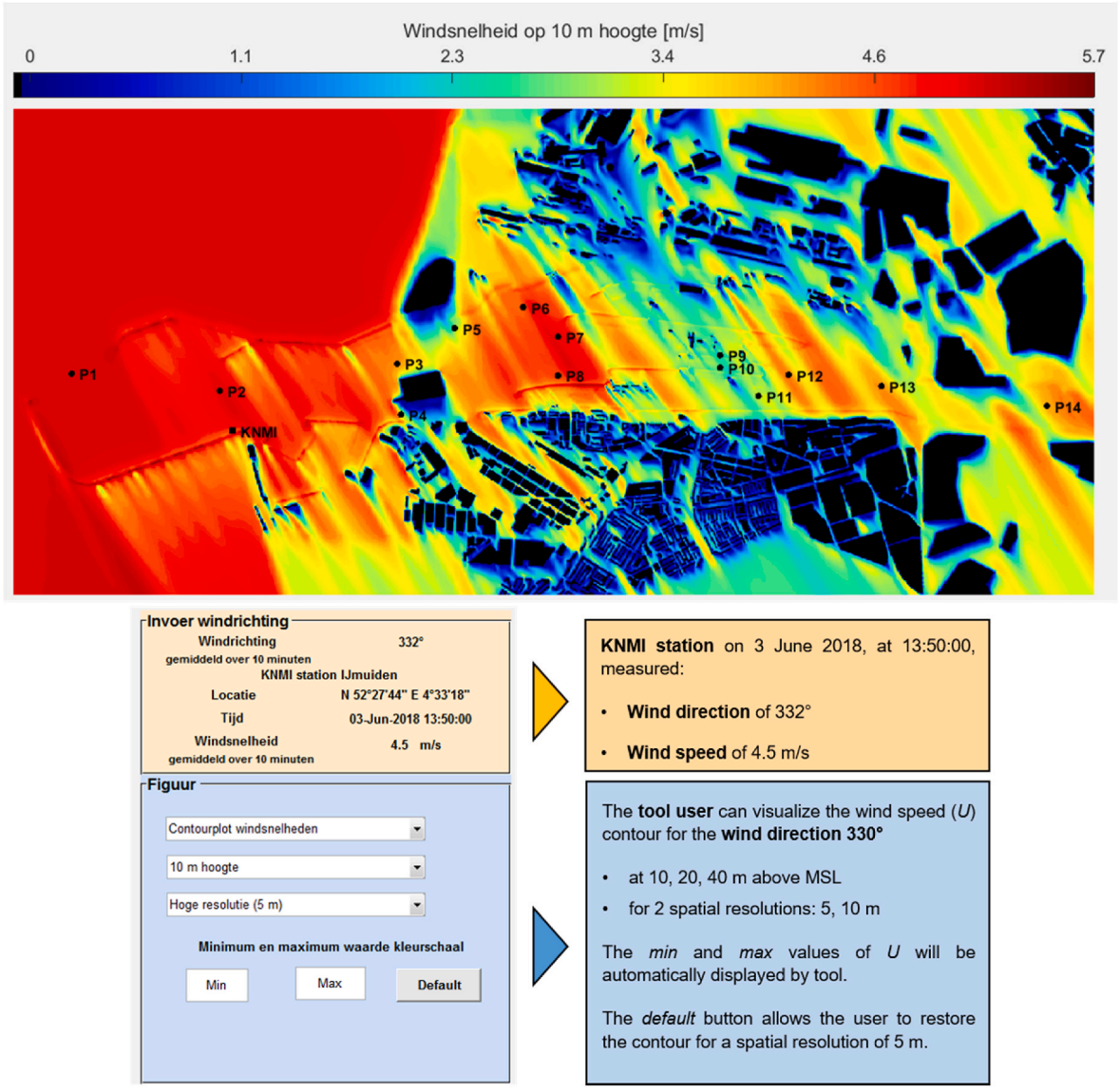

Fig. 12. As an example (June 3, 2018, 13:50:00): mean wind speed contours for wind direction 330°, at 10 m above MSL and with a spatial resolution of 10 m.

5.2. *The graphical interface of the tool*

The tool has a graphical user interface (GUI) composed of four panels and one main display to set options and visualize the results (Fig. 10). As also stressed in Section 5.1, only the area of interest including the new sea lock (of about 3 × 8 km^2, see also Fig. 5) is displayed in the tool to comply with the explicit requests of the client, i.e. the Port Authority of Amsterdam. To make the tool fully understandable for the tugboat pilots operating at this specific geographic location (in the Netherlands), the Dutch language was used. Note most options included in the tool were explicitly requested and agreed with the client based on specific needs.

The top-right yellow panel (*Invoer windrichting*, Fig. 11), not editable by the user, shows the 10-min average wind speed (*Windsnelheid*, m/s) and wind direction (*Windrichting*, in degrees) measured by the *KNMI* station with the indication of date and time (*Tijd*, DD-MM-YYYY HH:MM:SS) and geographical coordinates (*Locatie*) expressed in terms of Universal Transverse Mercator (UTM). The data are read by the tool by the FTP server every 10 min. In the middle-right blue panel (*Figuur*, Fig. 11), different options can be selected by the user to visualize (in the main display) the wind speed and turbulence intensity contours. The user ("User input" blocks in Fig. 9) can choose to display the wind speed contours *without* (*Countourplot windsnelheden*, Fig. 12) and *with* (*Countour en vectorplot*, Fig. 13) overlapping velocity vectors, at three different heights (*hoogte*: 10, 20, 40 m) above MSL and for two spatial resolutions (*resolutie*: 5, 10 m). As discussed in Section 5.1, the tool does not employ the CFD grid used to provide the information (see Fig. 6), but a regularly spatial domain built in MATLAB for the purpose. In the middle-right blue panel (*Figuur*, Fig. 11), once a set of contours are displayed by the user, the max and min values of the selected contour variables are automatically provided as well (*Minimum en maximum waarde kleurschaal*) by the tool. The *Default* button can be used to restore the default options, such as the contours without velocity vectors at 10 m above the MSL at a spatial resolution of 5 m. Alternatively, the user is free to change the display options (see the loop in Fig. 9). The options of the blue panel above described for the wind velocity apply also to the turbulence intensity variable (Fig. 14). The tool is also interactive and gives the possibility to the user of manually selecting (with the mouse) custom positions on the main display in order to get information on 10-min average wind speed (m/s), wind direction (in degrees) and turbulence intensity (%). This information is then displayed in the bottom-right green panel: *Windsnelheid* (wind speed), *Windrichting* (local wind direction), *Turbulentie-intensiteit* (turbulence intensity) (Figs. 10 and 11).

Finally, in the bottom pink panel (*Strategische punten*, Figs. 10, 11 and 15), the 10-min average wind speed (m/s), local wind direction (°) and

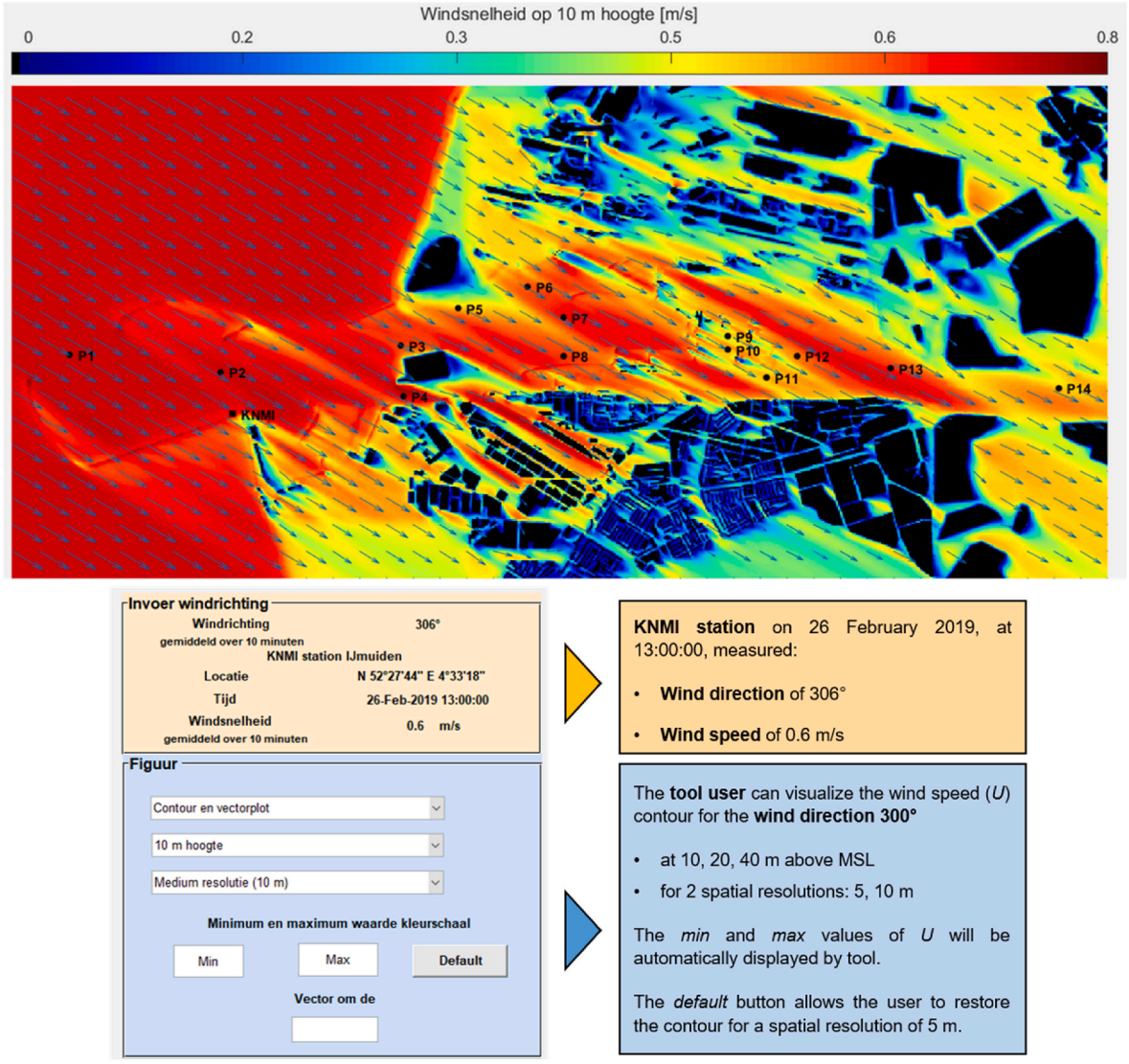

Fig. 13. As an example (February 26, 2019, 13:00:00): mean wind speed contours and mean velocity vectors for the wind direction 300°, at 10 m above MSL and a spatial resolution of 10 m.

turbulence intensity (%) values are displayed for 14 strategic positions (i.e. P1, …, P14) defined along the possible navigation routes of the seaport. The decision to add the pink panel was agreed with the client because large gradients of wind speed were observed during the validation (*step 3*, Fig. 4) along these routes both for Eastern and Western wind sectors, due to the presence of surrounding port infrastructures and buildings shielding the sea lock area (Ricci and Blocken, 2020). The bottom panel generally enables the tugboat pilots and the port stakeholders to better understand whether the access to the sea lock is advised in stormy weather. For example, for the *IJmuiden sea lock*, the distance between the entrance (P1) and the *new sea lock* (P10) is about 4 km (see Figs. 5 and 15). Considering that the maximum speed limit for large-size ships (e.g. containerships or a cruise ships) with draughts between 13.55 and 13.75 m in salt water (Port of Amsterdam, Art. 1, 2020) navigating through the North Sea Canal is of 3.2 knots (about 6 km/h), the time required to move from P1 to P10 would be of about 40 min. With the integrated tool, the tugboat pilots will be able to check about four times (wind updates available every 10 min) at each position P for possible changes in wind direction, wind speed and turbulence intensity occurring along the route.

6. Summary and conclusions

Seaports are important nodes and facilitate the worldwide trade volume via sea. In combination with waterways these are considered the entry and the exit points of a country's trade. The increasing globalization leads to a growing competition in global trade in which seaports and generally all the involved port infrastructures play a key role. The expanding capacity of seaports for competitiveness worldwide and accommodate bigger cruise ships and containerships can lead to an increased risk exposure. Besides the unquestionable and positive impact of seaports on the global economy, the increasing ship size can also cause larger wind forces, which make the navigation through these areas more complicated. A significant number of accidents on cruise ships, containerships, and port infrastructures have occurred in stormy weather were reported in recent years. However, despite many efforts towards the safety management of seaports and waterways, the accurate knowledge of local-scale wind conditions within such complex environments is still challenging. The CFD technique (by means of high-resolution computational geometries and grids) in combination with on-site measurements can be considered one of the most valid approaches in wind engineering research and practice to properly resolve the local-scale effects induced by obstacles. In the present paper an

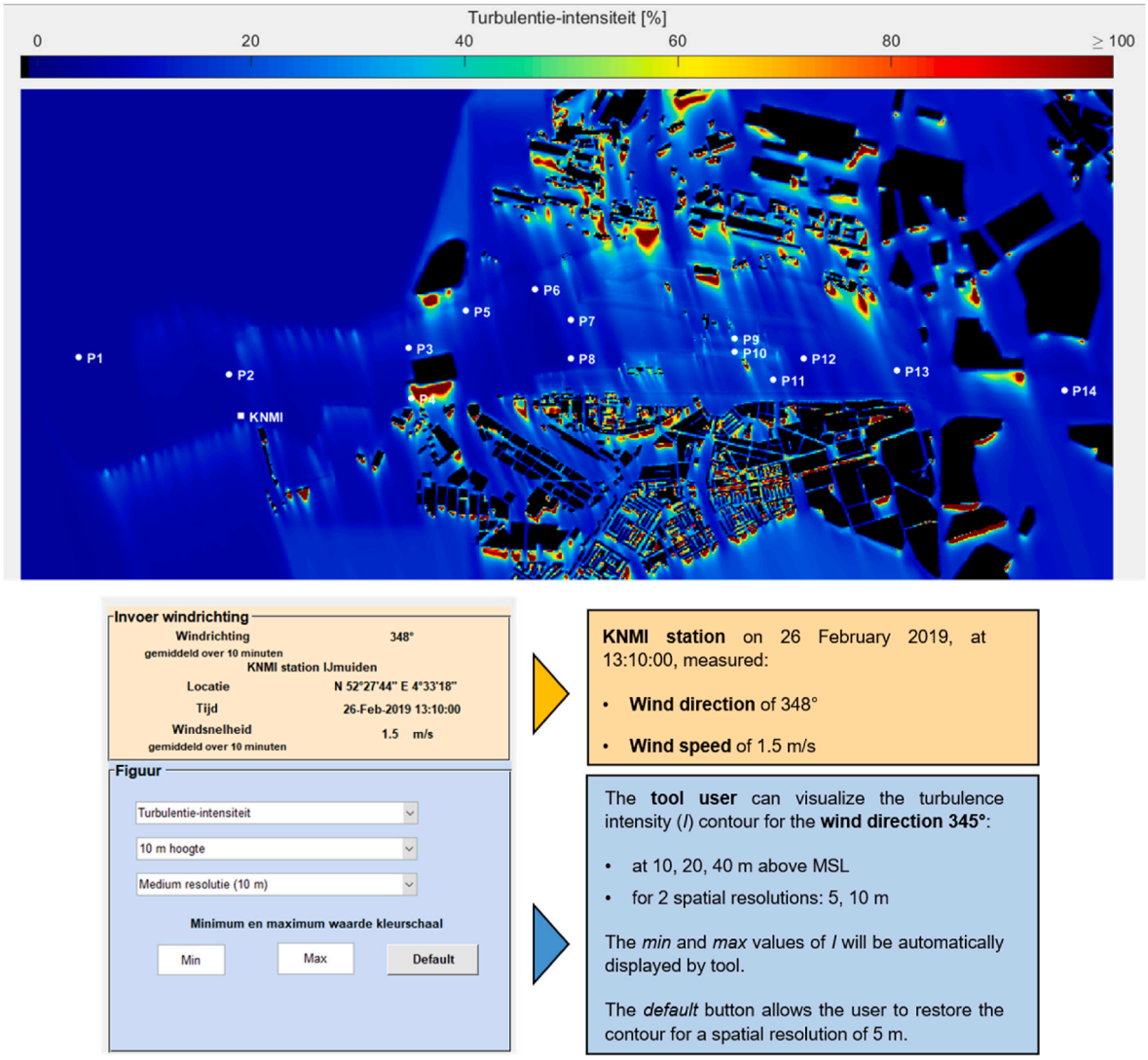

Fig. 14. As an example (February 26, 2019, 13:10:00): turbulence intensity contours for the wind direction 345° at 10 m above MSL and with a special resolution of 10 m.

innovative integrated tool (based on CFD simulations and on-site measurements), that provides the tugboat pilots and other port stakeholders with local-scale wind conditions in seaport areas, was developed. It was applied for the *new configuration* of the *IJmuiden sea lock* (Port of Amsterdam, the Netherlands) and the surrounding area, for which CFD simulations and on-site measurements already presented in the earlier publication by Ricci and Blocken (2020). Several limitations of this research study should be noted.

- In absence of temperature data, neutral atmospheric stability conditions were considered during the on-site measurements by selecting only events with a 10-min mean wind speed larger than 6 m/s (see also Ricci and Blocken, 2020).
- The storm events that occurred on 3 and January 18, 2018 caused technical damage to the anemometer stations *IJm2* and *IJm3* with a subsequent disruption of the network system and loss of data for several days. Thus, these extreme events could not be considered for the validation of CFD data.
- In line with several previous CFD studies (e.g. Carpentieri and Robins, 2015; Ricci et al., 2017; Paden et al., 2022), geometrical simplifications were applied to buildings, waterways, bridges and streets, given the high complexity of the area under investigation.
- The RANS approach might exhibit some limitations when predicting flow separation and flow reversal zones. More sophisticated approaches, as the large-eddy simulations, could have been used in this study. However, the absence of best practice guidelines and the larger computational costs (than RANS) to simulate 24 wind directions of a meso-γ scale model are considered as serious limitations (Blocken, 2018).
- Since the real-time measured wind direction at the *KNMI* station is not necessarily a multiple of 15°, the data employed for rescaling are those associated with the CFD simulation whose wind direction is the closest multiple of 15°. Although this can be considered as a limitation, an error of ±7.5° is still considered minor given the complexity of the seaport topography and the turbulent ABL flow.
- Although is an output of the software application, as mentioned in Section 5.1 the turbulence intensity was not rescaled according to the measured data since it was not explicitly requested by the KNMI as real-time output to support tugboat pilots that mainly interested in wind speed and direction.

Despite the aforementioned limitations, the project confirmed the importance of involving all port stakeholders at different levels (as port authorities and meteorological institutes) in order to develop a user-friendly integrated tool that allows recognizing possible *threats* when

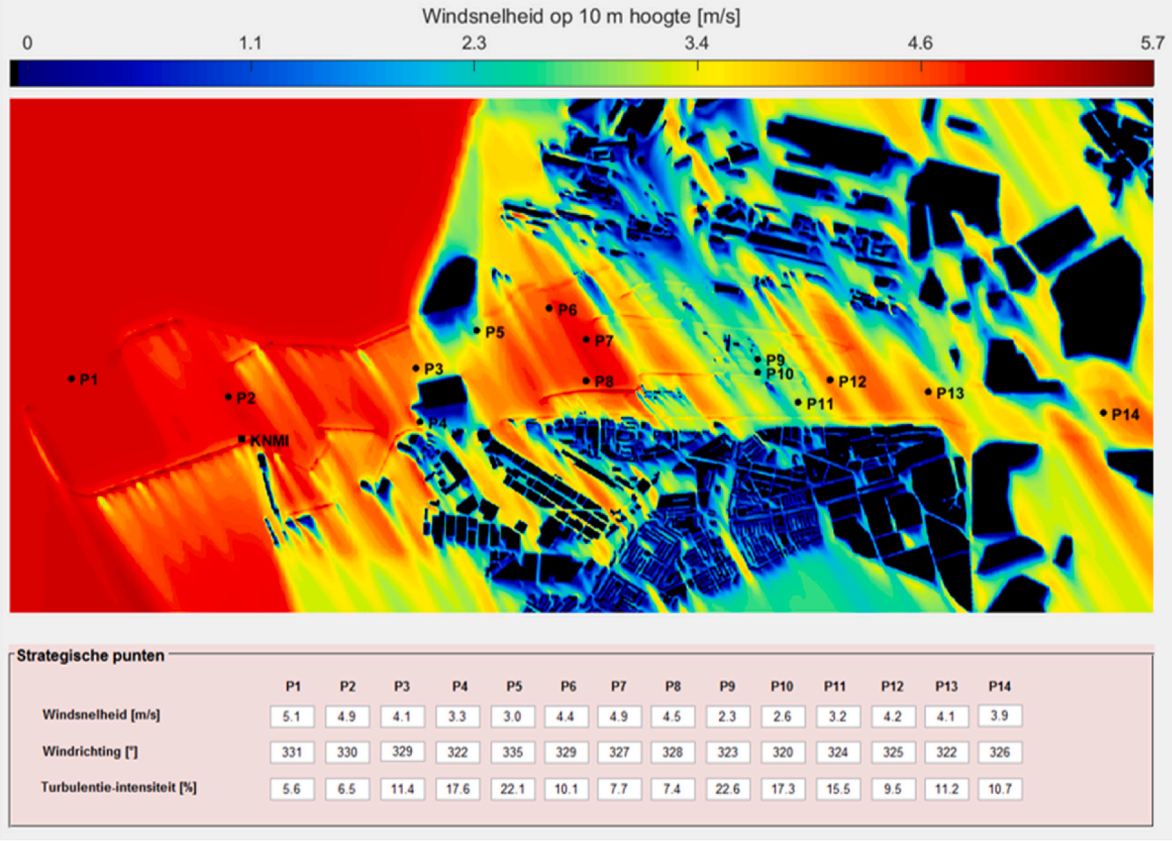

	P1	P2	P3	P4	P5	P6	P7	P8	P9	P10	P11	P12	P13	P14
Windsnelheid [m/s]	5.1	4.9	4.1	3.3	3.0	4.4	4.9	4.5	2.3	2.6	3.2	4.2	4.1	3.9
Windrichting [°]	331	330	329	322	335	329	327	328	323	320	324	325	322	326
Turbulentie-intensiteit [%]	5.6	6.5	11.4	17.6	22.1	10.1	7.7	7.4	22.6	17.3	15.5	9.5	11.2	10.7

Fig. 15. The bottom (pink) panel shows the mean wind speed (m/s), local wind direction (°) and turbulence intensity (%) values at 14 strategic positions defined along possible routes of navigation (at 10 m above MSL). As an example, the contour shows the mean wind speed associated with wind direction 330° at 10 m above MSL and with a spatial resolution of 10 m.

maneuvering ships in seaports and waterways. The 3D steady RANS approach was found to be a reasonable compromise between the available time (less than one year) to provide the partners with a tool to train the tugboat pilots and the accuracy required to detect potentially dangerous wind flow conditions at the *new sea lock*. As demonstrated in the earlier publication by (Ricci and Blocken, 2020) and stressed by review papers (e.g. Blocken, 2018), the 3D steady RANS approach showed a high reliability in identifying high wind speed regions potentially risky for ships maneuvering in these areas.

The integrated tool is versatile and allows a tugboat pilot maneuvering inside the *IJmuiden sea lock* to check and visually display the wind speed, direction, and turbulence intensity at each point of the map as well as by means of some pre-defined common ship routes. In particular, this option enables the tugboat pilot to choose the safest route and to stop maneuvering within a reasonable margin of time if necessary. Although some indications were provided about the ship routes, as explicitly required by the client, note that the ships themselves were not included in the CFD simulations. Similarly, any possible effect caused by the wind-wave interaction as well as non-synoptic winds (e.g. downbursts and tornadoes) were not accounted for in the present release of the tool. These items can be considered as follow-up implementations.

In conclusion, the tool represents the results of a cooperation between academicians and practitioners targeted at improving the awareness of risks and the prevention of detrimental accidents in seaport areas during stormy days.

CRediT authorship contribution statement

A. Ricci: Writing – review & editing, Methodology, numerical and experimental, Investigation, Software, development, Conceptualization. **R. Vasaturo:** Writing – review & editing, Methodology, Software, development, Conceptualization. **B. Blocken:** Writing – review & editing, Supervision, Conceptualization, Project administration.

Declaration of competing interest

The authors declare that they have no known competing financial interests or personal relationships that could have appeared to influence the work reported in this paper.

Data availability

Data will be made available on request.

Acknowledgements

The authors gratefully acknowledge the Koninklijk Nederlands Meteorologisch Instituut (KNMI) and the Port Authority of Amsterdam for the collaboration. The authors also gratefully acknowledge the partnership with ANSYS CFD. Alessio Ricci was a postdoctoral fellow of the Research Foundation – Flanders (FWO) (project FWO 1256822N) at the time of writing the article and its financial support is gratefully acknowledged.

References

Albers, R.A.W., Bosch, P.R., Blocken, B., van den Dobbelsteen, A.A.J.F., van Hove, L.W. A., Spit, T.J.M., van de Ven, F., van Hooff, T., Rovers, V., 2015. Overview of challenges and achievements in the climate adaptation of cities and in the climate proof cities program. Build. Environ. 83, 1–10.

Almaz, A.O., Or, I., Özbaş, B., 2006. Investigation of transit maritime traffic in the strait of Istanbul through simulation modeling and scenario analysis. Int. J. Simulat. Syst. Sci. Technol. 7, 1–9.
ANSYS Fluent, 2013. Release 16.0, Theory Guide. ANSYS Inc, Canonsburg.
Bailey, N., Ellis, N., Sampson, H., 2008. Training and Technology Onboard Ship: How Seafarers Learned to Use the Shipboard Automatic Identification System (AIS). Lloyd's Register Educational Trust Research Unit. Seafarers International Research Centre, and Cardiff University, Cardiff.
Baker, C.J., 2007. Wind engineering – past, present and future. J. Wind Eng. Ind. Aerod. 95, 843–870.
BBC News, 2018. URL: https://www.bbc.com/news/world-europe-42731505. (Accessed 16 November 2021).
BBC News, 2021. URL: https://www.bbc.com/news/world-middle-east-56505413. (Accessed 16 November 2021).
Becker, A.H., Matson, P., Fischer, M., Mastrandrea, M.D., 2015. Towards seaport resilience for the climate change adaptation: stakeholder perceptions of hurricane impacts in Gulfport (MS) and Providence (RI). Prog. Plann. 99, 1–49.
Blocken, B., 2014. 50 years of computational wind engineering: past, present and future. J. Wind Eng. Ind. Aerod. 129, 69–102.
Blocken, B., 2015. Computational Fluid Dynamics for Urban Physics: importance, scales, possibilities, limitations and ten tips and tricks towards accurate and reliable simulations. Build. Environ. 91, 219–245.
Blocken, B., 2018. LES over RANS in building simulation for outdoor and indoor applications: a foregone conclusion? Build. Simulat. 11, 821–870.
Blocken, B., Gualtieri, C., 2012. Ten iterative steps for model development and evaluation applied to computational fluid dynamics for environmental fluid mechanics. Environ. Model. Software 33, 1–22.
Blocken, B., Stathopoulos, T., Carmeliet, J., 2007a. CFD simulation of the atmospheric boundary layer: wall function problems. Atmos. Environ. 41, 238–252.
Blocken, B., Carmeliet, J., Stathopoulos, T., 2007b. CFD evaluation of wind speed conditions in passages between parallel buildings - effect of wall-function roughness modifications for the atmospheric boundary layer flow. J. Wind Eng. Ind. Aerod. 95, 941–962.
Blocken, B., van der Hout, A., Dekker, J., Weiler, O., 2015. CFD simulation of wind flow over natural complex terrain: case study with validation by field measurements for Ria de Ferrol, Galicia, Spain. J. Wind Eng. Ind. Aerod. 147, 43–57.
Britter, R., Schatzmann, M., 2007. Model Evaluation Guidance and Protocol Document COST Action 732. COST Office Brussels, Belgium, ISBN 3-00-018312- 4.
Burlando, M., Freda, A., Ratto, C.F., Solari, G., 2010. A pilot study of the wind speed along the Rome–Naples HS/HC railway line. Part1 – numerical modelling and wind simulations. J. Wind Eng. Ind. Aerod. 98, 392–403.
Burlando, M., De Gaetano, P., Pizzo, M., Repetto, M.P., Solari, G., Tizzi, M., 2013. Wind climate analysis in complex terrains. J. Wind Eng. Ind. Aerod. 123, 349–362.
Burlando, M., Pizzo, M., Repetto, M.P., Solari, G., De Gaetano, P., Tizzi, M., 2014. Short-term wind forecast for the safety management of complex areas during hazardous wind events. J. Wind Eng. Ind. Aerod. 135, 170–181.
Cao, X., Lam, J.S.L., 2018. Simulation-based catastrophe-induced port loss estimation. Reliab. Eng. Syst. Saf. 175, 1–12.
Carpentieri, M., Robins, A.G., 2015. Influence of urban morphology on air flow over building arrays. J. Wind Eng. Ind. Aerod. 145, 61–74.
Casey, M., Wintergerste, T., 2000. Best Practice Guidelines, ERCOFTAC Special Interest Group on Quality and Trust in Industrial CFD. ERCOFTAC, Brussels.
Cebeci, T., Bradshaw, P., 1997. Momentum Transfer in Boundary Layers. Hemisphere Publishing Corporation, New York, ISBN 0070103003.
Chen, C., Shiotani, S., Sasa, K., 2015. Effect of ocean currents on ship navigation in the east China sea. Ocean Eng. 104, 283–293.
Chen, C., Sasa, K., Ohsawa, T., Kashiwagi, M., Prpić-Oršić, J., Mizojiri, T., 2020. Comparative assessment of NCEP and ECMWF global datasets and numerical approaches on rough sea ship navigation based on numerical simulation and shipboard measurements. Appl. Ocean Res. 101, 102219.
Cho, H.S., Lee, J.S., Moon, H.C., 2018. Maritime risk in seaport operation: a cross-country Empirical Analysis with theoretical foundations. Asian J. Shipping. Logistic. 34, 240–247.
Darbra, R.M., Casal, J., 2004. Historical analysis of accidents in seaports. Saf. Sci. 42, 85–98.
European Commission, 2021. URL: https://ec.europa.eu/inea/en/connecting-europe-facility. (Accessed 16 November 2021).
Franke, J., Hellsten, A., Schlünzen, H., Carissimo, B., 2007. Best Practice Guideline for the CFD Simulation of Flows in the Urban Environment. COST Office Brussels, ISBN 3-00-018312-4.
Gao, X., Makino, H., Furusho, M., 2015. Analysis of ship drifting in a narrow channel using Automatic Identification System (AIS) data. WMU J. Maritime Aff. 16, 351–363.
Gharehgozli, A.H., Adams, J.M.A., von Zharen, W., 2017. Evaluating a "wicked problem": a conceptual framework on seaport resiliency in the event of weather disruptions. Technol. Forecast. Soc. Change 121, 65–75.
Gomez Paz, M.A., Camarero Orive, A., González Cancelas, N., 2015. Use of the Delphi method to determine the constraints that affect the future size of large container ships. Marit. Pol. Manag. 42 (3), 263–277.
Gunnar Aarsæther, K., Moan, T., 2009. Estimating navigation patterns from AIS. J. Navig. 62, 587–607.
Hanjalic, K., 2005. Will RANS survive LES? A view of perspectives. J. Fluid Eng. 127, 831–839.
Harati-Mokhtari, A., Wall, A., Brooks, P., Wang, J., 2007. Automatic identification system (AIS): data reliability and human error implications. J. Navig. 60, 373–389.
HetLegioen, 2018. URL: https://www.youtube.com/watch?v=uXmw0wEiGec. (Accessed 16 November 2021).
Hiroshi, K., Kenichi, K., Hideo, O., Takuro, I., Ichiro, A., Ryo, Y., Hisafumi, Y., Tomohiro, R., Yuji, A., Kosuke, K., Seiji, I., Shota, Y., Hideaki, A., Shuji, M., 2022. CFD assessment of the wind forces and moments of superstructures through RANS. Appl. Ocean Res. 103364, 129.
Hsieh, C.H., Tai, H.H., Lee, Y.N., 2014. Port vulnerability assessment from the perspective of critical infrastructure interdependency. Marit. Pol. Manag. 41 (6), 589–606.
Insider, 2019. URL: https://www.insider.com/cruise-ship-nearly-plows-into-venice-cafe-during-a-storm-2019-7. (Accessed 16 November 2021).
International Transport Forum (ITF), 2015. The Impact of Mega-Ships. International Transport Forum Policy Papers, No. 10. OECD Publishing, Paris.
Iseki, T., 2019. Real-time estimation of the ship manoeuvrable range in wind. Ocean Eng. 190, 106396.
Janssen, W.D., Blocken, B., van Wijhe, H.J., 2017. CFD simulations of wind loads on a container ship: validation and impact of geometrical simplifications. J. Wind Eng. Ind. Aerod. 166, 106–116.
Jian, W., Liu, C., Lee Lam, S.J., 2019. Cyclone risk model and assessment for East Asian container ports. Ocean Coast Manag. 178, 104796.
Kang, L., Meng, Q., Zhou, C., Gao, S., 2019. How do ships pass through L-shaped turnings in the Singapore strait? Ocean Eng. 182, 329–342.
Kfw, 2021. URL: https://www.kfw.de/stories/economy/infrastructure/sluice-ijmuiden/. (Accessed 16 November 2021).
KNMI, 2018. URL: https://www.knmi.nl/kennis-en-datacentrum/achtergrond/code-rood-voor-zeer-zware-windstoten-op-18-januari-2018. (Accessed 16 November 2021).
Kolios, S., Stylios, C., Petunin, A., 2015. AWebGIS platform to monitor environmental conditions in ports and their surroundings in South Eastern Europe. Environ. Monit. Assess. 187, 574.
Kortcheva, A., Galabov, V., Marinski, J., Andreac, V., Stylios, C., 2018. New approaches and mathematical models for environmental risk management in seaports. IFAC-PapersOnLine 51 (30), 366–371.
Kron, W., 2013. Coasts: the high-risk areas of the world. Nat. Hazards 66, 1363–1382.
Kron, W., Löw, P., Kundzewicz, Z.W., 2019. Changes in risk of extreme weather events in Europe. Environ. Sci. Pol. 100, 74–83.
Launder, B.E., Spalding, D.B., 1974. The numerical computation of turbulent flows. Comput. Methods Appl. Mech. Eng. 3, 269–289.
Leckebusch, G.C., Ulbrich, E., 2004. On the relationship between cyclones and extreme windstorm events over Europe under climate change. Global Planet. Change 44, 181–193.
Maritime Security Regime Concept, 2012. A global approach to regional challenges. URL: https://apps.dtic.mil/sti/citations/ADA587463. (Accessed 16 November 2021).
Mathworks, 2016. Global Optimization Toolbox: User's Guide. release, 2016b.
McIntosh, R.D., Becker, A., 2019. Expert evaluation of open-data indicators of seaport vulnerability to climate and extreme weather impacts for U.S. North Atlantic ports. Ocean Coast Manag. 180, 104911.
Merrick, J.R.W., van Dorp, J.R., Blackford, J.P., Shaw, G.L., Harrald, J., Mazzuchi, T.A., 2003. A traffic density analysis of proposed ferry service expansion in San Francisco Bay using a maritime simulation model. Reliab. Eng. Syst. Saf. 81, 119–132.
Mirror, Mumbai, 2020. URL: https://mumbaimirror.indiatimes.com/mumbai/other/3-high-capacity-cranes-crash-at-jnpt/articleshow/77383192.cms. (Accessed 16 November 2021).
Mori, N., Takemi, T., 2016. Impact assessment of coastal hazards due to future changes of tropical cyclones in the North Pacific Ocean. Weather Clim. Extrem. 11, 53–69.
Neumann, B., Vafeidis, A.T., Zimmermann, J., Nicholls, R.J., 2015. Future coastal population growth and exposure to sea-level rise and coastal flooding - a global assessment. PLoS One 10 (3), e0118571.
Paden, I., García-Sánchez, C., Ledoux, H., 2022. Towards automatic reconstruction of 3D city models tailored for urban flow simulations. Front. Built Environ. https://doi.org/10.3389/fbuil.2022.899332.
Pasquill, F., 1961. The estimation of the dispersion of windborne material. Meteorol. Mag. 90, 33–49.
Pelling, M., 2003. The Vulnerability of Cities: Natural Disasters and Social Resilience, first ed. (Earthscan, London).
Population Reference Bureau, 2003. Ripple Effects: Population and Coastal Regions Measure Communication, 1875 Connecticut Ave., NW. Suite 520, Washington, DC 20009 USA.
Port of Amsterdam, 2020. Art. 1. URL: https://www.portofamsterdam.com/en/announcement/adoption-maximum-speed-north-sea-canal-and-afgesloten-ij-until-stenen-hoofd-amsterdam. (Accessed 16 November 2021).
Port of Amsterdam, 2021. New sea lock. URL: https://www.portofamsterdam.com/en/discover/new-sea-lock. (Accessed 16 November 2021).
Prpic-Orsic, O., Valčič, M., Čarija, Z., 2020. A hybrid wind load estimation method for container ship based on computational fluid dynamics and neural networks. J. Mar. Sci. Eng. 8 (7), 539.
Repetto, M.P., Burlando, M., Solari, G., De Gaetano, P., Pizzo, M., 2017. Integrated tools for improving the resilience of seaports under extreme wind events. Sustain. Cities Soc. 32, 277–294.
Repetto, M.P., Burlando, M., Solari, G., De Gaetano, P., Pizzo, M., Tizzi, M., 2018. A web-based GIS platform for the safe management and risk assessment of complex structural and infrastructural systems exposed to wind. Adv. Eng. Software. 117, 29–45.
Ricci, A., Blocken, B., 2020. On the reliability of the 3D steady RANS approach in predicting microscale wind conditions in seaport areas: the case of the IJmuiden sea lock. J. Wind Eng. Ind. Aerod. 207, 104437.

Ricci, A., Kalkman, I., Blocken, B., Burlando, M., Freda, A., Repetto, M.P., 2017. Local-scale forcing effects on wind flows in an urban environment: impact of geometrical simplifications. J. Wind Eng. Ind. Aerod. 170, 238–255.
Ricci, A., Kalkman, I., Blocken, B., Burlando, M., Freda, A., Repetto, M.P., 2018. Large-scale forcing effects on wind flows in the urban canopy: impact of inflow conditions. Sustain. Cities Soc. 42, 593–610.
Ricci, A., Janssen, W.D., van Wijhe, H.J., Blocken, B., 2020. CFD simulation of wind forces on ships in ports: case study for the Rotterdam Cruise Terminal. J. Wind Eng. Ind. Aerod. 205, 104315.
Ricci, A., Guasco, M., Caboni, F., Orlanno, M., Giachetta, A., Repetto, M.P., 2022. Impact of surrounding environments and vegetation on wind comfort assessment of a new tower with vertical green park. Build. Environ. 207, 108409.
Rodrigue, J.P., Notteboom, T., 2009. The terminalization of supply chains: reassessing the role of terminals in port/hinterland logistical relationships. Marit. Pol. Manag. 36 (2), 165–183.
Rong, H., Teixeira, A.P., Guedes Soares, C., 2019. Ship trajectory uncertainty prediction based on a Gaussian Process model. Ocean Eng. 182, 499–511.
Ronza, A., Lázaro-Touza, L., Carol, S., Casal, J., 2009. Economic valuation of damages originated by major accidents in port areas. J. Loss Prev. Process. Ind. 22, 639–648.
Shih, T.H., Liou, W.W., Shabbir, A., Zhu, J., 1995. A new k-ε eddy-viscosity model for high Reynolds number turbulent flows e model development and validation. Comput. Fluid. 24, 227–238.
Shipping Watch, 2019. URL: https://shippingwatch.com/Ports/article11812720.ece. (Accessed 16 November 2021).
Solari, G., Repetto, M.P., Burlando, M., De Gaetano, P., Pizzo, M., Tizzi, M., Parodi, M., 2012. The wind forecast for safety management of port areas. J. Wind Eng. Ind. Aerod. 104–106, 266–277.
Stathopoulos, T., 2002. The numerical wind tunnel for industrial aerodynamics: real or virtual in the new millennium? Wind Struct. 5, 193–208.
Stull, R.B., 1988. An Introduction to Boundary Layer Meteorology, first ed. Springer Netherlands, ISBN 978-94-009-3027-8.
Sys, C., Blauwens, G., Omey, E., Van De Voorde, E., Witlox, F., 2008. In search of the link between ship size and operations. Transport. Plann. Technol. 31 (4), 435–463.
Taramelli, A., Valentini, E., Sterlacchini, S., 2015. A GIS-based approach for hurricane hazard and vulnerability assessment in the Cayman Islands. Ocean Coast Manag. 108, 116–130.
Tominaga, Y., Mochida, A., Yoshie, R., Kataoka, H., Nozu, T., Yoshikawa, M., et al., 2008. AIJ guidelines for practical applications of CFD to pedestrian wind environment around buildings. J. Wind Eng. Ind. Aerod. 96, 1749–1761.
Torre, S., Burlando, M., Ruscelli, D., Repetto, M.P., Camauli, G., 2021. Wind tunnel experimental investigation of the aerodynamic coefficients reduction due to sheltering surroundings on a cruise ship moored in port. J. Wind Eng. Ind. Aerod. 218, 104731.
Ulbrich, U., Leckebusch, G.C., Pinto, J.G., 2009. Extra-tropical cyclones in the present and future climate: a review. Theor. Appl. Climatol. 96, 117–131.
UNCTAD, 2011. Ad Hoc Expert Meeting on Climate Change Impacts and Adaptation: a Challenge for Global Ports-Main Outcomes and Summary of Discussions.
UNCTAD/RTM, 2018. In: United Conference on Trade and Development. Review of Maritime Transport, ISBN 978-92-1-112928-1.
Vairetti, C., González-Ramírez, R.G., Maldonado, S., Álvarez, C., Voβ, S., 2019. Facilitating conditions for successful adoption of inter-organizational information systems in seaports. Transport. Res. Part A 130, 333–350.
van Dongeren, A., Ciavola, P., Martinez, G., Viavattene, C., Bogaard, T., Ferreira, O., Higgins, R., McCall, R., 2018. Introduction to RISC-KIT: resilience-increasing strategies for coasts. Coast Eng. 134, 2–9.
van Hooff, T., Blocken, B., 2010. Coupled urban wind flow and indoor natural ventilation modelling on a high-resolution grid: a case study for the Amsterdam ArenA stadium. Environ. Model. Software 25, 51–65.
Vasaturo, R., Kalkman, I., Blocken, B., Wesemael, P.J.V., 2018. Large eddy simulation of the neutral atmospheric boundary layer: performance evaluation of three inflow methods for terrains with different roughness. J. Wind Eng. Ind. Aerod. 173, 241–261.
Wieringa, J., 1992. Updating the Davenport roughness classification. J. Wind Eng. Ind. Aerod. 41–44, 357–368.
Wolfgang, K., 2013. Coast: the high-risk areas of the world. Nat. Hazards 66, 1363–1382.
Yip, T.L., 2008. Port traffic risks – a study of accidents in Hong Kong waters. Transport. Res. Part E 44, 921–931.
Yoo, J.H., Schrijvers, P., Koop, A., Park, J.C., 2022. CFD prediction of wind loads on FPSO and shuttle tankers during side-by-side offloading. J. Mar. Sci. Eng. 10 (5), 654.
Zhang, Y., Lam, S.J.L., 2015. Estimating the economic losses of port disruption due to extreme wind events. Ocean Coast Manag. 116, 300–310.
Zhang, Y., Lam, S.J.L., 2016. Estimating economic losses of industry clusters due to port disruptions. Transport. Res. Pol. Pract. 91, 17–33.
Zhou, Y., Daamen, W., Vellinga, T., Hoogendoorn, S.P., 2020. Impacts of wind and current on ship behavior in ports and waterways: a quantitative analysis based on AIS data. Ocean Eng. 213, 107774.